Investigation of Mooring Breakage Impact on Dynamic Responses of a 15MW Floating Offshore Wind Turbine

Debang NIE [a], Yang YANG [a,*], Shuai LI [b,*], Jie YU [c], Musa BASHIR [d], Jiaqing YIN [a], Yajun REN [b], Jungang HAO [b], Fuqiang WANG [b], Qianni LIU [a], Chun LI [c]

[a.] Faculty of Maritime and Transportation, Ningbo University, Ningbo, 315211, P.R. China

[b.] China Renewable Energy Engineering Institute, Beijing 100120, China

[c.] School of Energy and Power Engineering, University of Shanghai or Science and Technology, Shanghai 200093, China

[d.] Department of Civil and Environmental Engineering, University of Liverpool, Brownlow Hill, Liverpool, L697ZX, United Kingdom

Abstract: The stability and integrity of the mooring system are some of critical factors affecting the safety and performance of floating offshore wind turbines (FOWTs). For this reason, it is necessary to investigate the dynamic responses of the rotor, platform, and the remaining cables of the FOWT subjected to mooring breakages. This is because a mooring breakage significantly increases the risk of damage to the FOWT, especially for a nonredundant mooring system. This study has analyzed the platform motions and mooring tension of a 15MW FOWT, where each offset column connects to two and three mooring lines to enhance the redundancy of the mooring system. The fully coupled simulations of the FOWTs under mooring breakage scenarios are examined using the well-validated numerical framework, OpenF2A, to consider wind, wave and current loading combinations. The result reveals that the breakage of a single mooring has a minor impact on the aerodynamic performance and aeroelastic response of the FOWT for both mooring system configurations. Notably, the platform experiences significant surge and sway when the upwind mooring breaks, leading to a sharp increase in tension of the remaining mooring lines positioned in the same direction. Moreover, the occurrence of snap load events is another factor resulting in the abrupt increase in the mooring tension. However, the maximum tension in the remaining mooring lines has not exceeded the threshold of breaking stress for both redundant mooring systems. The mooring configuration with two catenary cables connected to each column is suggested for the station-keeping system of the 15MW FOWT considering the dynamic behavior and manufacture cost.

Keywords: Floating offshore wind turbine; Mooring breakage; Fully coupled analysis; Dynamic behavior; OpenF2A.

* corresponding author: Yang Yang: yangyang1@nbu.edu.cn; Shuai Li: shuai-li16@mails.tsinghua.edu.cn

1 Introduction

Offshore wind energy offers a compelling array of advantages, ranging from abundant renewable resource availability and enhanced energy potential to environmental sustainability and economic benefits [1]. Therefore, offshore wind energy technology has experienced rapid development over the past decade. The annual wind report released by the Global Wind Energy Council (GWEC) illustrates that global cumulative wind power capacity passed the first 1TW milestone in 2023 [2]. Approximately 80% of the exploitable wind energy resources are located in deep offshore waters [3], providing a natural advantage for the development of Floating Offshore Wind Turbines (FOWT). Thus, studying FOWT is essential for advancing offshore wind energy technology, improving turbine performance, and ensuring the sustainable development of offshore wind farms. It is worth noting that mooring system is an essential component that significantly influence the stability of FOWT [4].

Semi-submersible platform is widely deployed in the pioneering demonstration and commercial floating wind projects over the world due to their advantages including widely applicable range of water depth, good hydrodynamic performance, and relatively simple installation and transportation process [5]. The floating platform provides essential assurance for the whole structure of a FOWT remains afloat and stable [6]. Due to higher wave and current energy density, the floating structure experiences motion and hydrodynamic loads that can significantly influence the power performance by transferring these loads to the wind turbine [7-8]. Meanwhile, it is noted that the fluctuation in platform motions significantly affect the aerodynamic performance and structural dynamics of the FOWT [9-10], which brings new challenges for the mooring system too [11-12].

The mooring lines acting as the station keeping system are crucial to the safety of the platform and wind turbine structures. The mooring system is susceptible to failure resulting from corrosion, intense wind gusts, extreme wave conditions, or fatigue damage [13]. Additionally, accidental load scenarios (*e.g.* ship collisions) may cause mooring line failures. The dynamic response of the platform will be more intense due to the accidental loads. This will increase the possibility of a continuous breakage in the remaining mooring lines, which leads to a more serious consequence. Therefore, it is imperative to investigate the mooring breakage effects on the dynamic responses of FOWTs. Typically, the platform is expected to suffer a severely transient behavior in the event of a sudden mooring failure. This is especially critical when there is a rapid increase in translational motions following the mooring breakage that threatens the safety of the power cables. Furthermore, the tension in the remaining mooring lines may exceed the material strength limit, escalating the risk of more

severe accidents or even triggering collisions with adjacent wind turbines. Consequently, it is imperative to investigate the impact of mooring breakage on the dynamic response of FOWT platforms subjected to wind, wave, and current loadings [14].

Numerous studies have been conducted to examine the impact of mooring failure of oil/gas production platforms and floating wind platforms. Yang *et al*. [15-17] conducted an analysis to obtain the transient response of a coupled hull–tendon–riser leg platform (TLP) when the tension leg was suddenly disconnected due to an accident. The transient response and tension were compared and discussed from the perspective of system robustness. A quasi-static catenary model was employed to predict the tension in the mooring. Li *et al*. [18] devised a time-domain coupled dynamic model to examine the transient response of wind turbines on Spar platforms after an abrupt mooring failure. Their study unveiled significant transient responses of wind turbines in the event of mooring failures. Bai *et al*. [19] developed a numerical model of a semi-submersible platform and mooring system using ANSYS/AQWA software package for hydrodynamic analysis. The impact of a single mooring line failure on the platform motions was examined. It was found that the maximum tension in the mooring line was increased up to 18.07% while the reliability of the mooring line decreased by a maximum factor of 146.16 resulting from the mooring fracture. Ren *et al*. [20] conducted simulations using FAST and WAMIT numerical tools to analyze the dynamic response of a 5 MW TLP FOWT during a single mooring failure. The research results revealed a significant response from the FOWT, with an average safety factor for mooring of 2.04, which meets the recommended values of design standards. Ma *et al*. [21] investigated the impact of one single mooring line failure on the motion of a semi-submersible platform under extreme wind gust conditions. The study revealed that the FOWT experienced a horizontal drift over 300 meters in the mooring failure scenario, which could cause a fatal threat to other floating offshore structures or adjacent FOWTs. Yang et al. [22] calculated the dynamic response of a DeepCWind FOWT using a fully nonlinear model. It was found that the platform pitch achieves the peak value after the FOWT reaches a new equilibrium state following the mooring breakage. Bae *et al*. [23] analyzed the fracture impact of a mooring line on the performance of a 5MW semi-submersible FOWT. Numerical simulations conducted using an in-house integrated tool CHARM3D-FAST showed that mooring line failure led to a significant nacelle-yaw error and large platform drift. This results in risks of power cable disconnection and potential consecutive failures in neighboring FOWTs due to collisions. Wu *et al*. [24] employed FAST to investigate the transient dynamic response of the WindStar TLP wind turbine following the failure of a single

mooring line. The study found that when the mooring failure did not align with the wave direction, both the lateral motion of the wind turbine and the nacelle acceleration increase significantly. Subbulakshmi *et al*. [25] used a tuned mass damper (TMD) to explore the application of the transient response of FOWT during the mooring line failure. The huge platform drift caused by the mooring breakage as revealed in the above studies is mainly attributed to the non-redundant configuration mooring system that limits the platform motion in an orientation with only one cable.

He *et al*. [26] studied the slack-taut phenomena in the mooring cables of the NREL 5MW FOWT caused by the transient behavior under mooring breakage scenarios. The influence of single or multiple mooring failures on cable tensions was assessed. A method was also proposed for detecting mooring line failures. Piscopo and Scamardella [27] explored the influence of cost and system dynamics for both 3 (non-redundant) and 9 (redundant) moorings of the OC4 semi-submersible FOWT under ultimate, fatigue, and accidental loadings. Niranjan *et al*. [28] used OpenFAST [29] to study the dynamic response of a 15 MW FOWT under non-redundant and redundant mooring systems during mooring line breakage. Their analysis focused on a single mooring line failure, revealing that the FOWT with a 6-line mooring system exhibited reduced platform drift compared to the 3-line system and no obvious risk of additional mooring line breaking was observed. It is worth noting that Yang *et al*. [14] developed a fully coupled simulation model based on OpenFAST and ANSYS (OpenF2A) and investigated the impact of mooring breakage on the dynamic response of the NREL 5 MW ITI barge platform. However, the existing research on the extreme conditions and mooring failure of large wind turbines is still relatively limited. In order to address the energy demands, it is essential to investigate the dynamic response of FOWT and the variation in mooring tension under mooring failure conditions.

To address the limitations of the above studies, this paper proposes a fully coupled simulation model by incorporating OpenFAST with AQWA. The impact of mooring line breakage on the platform motion and mooring line tension of a 15MW semi-submersible FOWT is examined for two redundant mooring systems. Meanwhile, this study explores the impacts of single mooring line failures with a subsequent comparison of the results. Additionally, the transient effects caused by a sudden breakage of mooring line are investigated.

The redundant mooring system configuration is proposed following the description of IEA 15MW wind turbine model and VolturnUS-S platform in the next section. The fully coupled analysis framework based on OpenFAST and AQWA is presented and validated in Section 3. In Section 4, the

dynamic responses of the platform and mooring system under different mooring breakage scenarios are presented and discussed. Finally, Section 5 summarizes the main findings and conclusions of this study.

2 Description of the wind turbine model

2.1 The IEA 15MW wind turbine and semi-submersible platform

The reference 15MW wind turbine is designed by the International Energy Agency [30] for application in different offshore locations. This reference wind turbine is a Class IB direct-drive machine with a rotor diameter of 240m and a hub height of 150m. The DTU FFA-W3 airfoils series were used because of their publicly available polars and geometries. The main design parameters of the IEA 15MW wind turbine are presented in Table 1.

Table 1: Summary of the properties of the IEA 15MW wind turbine

Property	Value	Units
Rated power	15	MW
Blade tip speed ratio	9	-
Rotor diameter	240	M
Airfoils	FFA-W3	-
Hub height	150	M
Hub diameter	7.94	M
Blade mass	65	T
RNA mass	1017	T
Tower mass	860	T

The VolturnUS-S semi-submersible floating platform designed by the University of Maine to support the 15MW wind turbine is selected for the case study. The steel-made platform deployed in 200m water depth is comprised of one central column and three offset columns. Each of the offset columns connects one catenary mooring line in the initial design. The platform has a draft of 20m. The displacement volume of the undisplaced platform is 20206m^3 of seawater. The parameters of the VolturnUS-S semi-submersible floating platform are presented in Table 2. The IEA 15MW FOWT model is presented in Fig. 1.

Table 2: Summary of the properties of the VolturnUS-S

Property	Value	Units
Hull displacement	20,206	m^3
Draft	20	m

Mass	11783.9	t
Center of mass	[0.0, 0.0, -14.94]	m
Center of buoyancy	[0.0, 0.0, -13.63]	m
Roll Inertia	1.251×10^{10}	$kg\cdot m^2$
Pitch Inertia	1.251×10^{10}	$kg\cdot m^2$
Yaw Inertia	2.376×10^{10}	$kg\cdot m^2$
Water depth	200	m

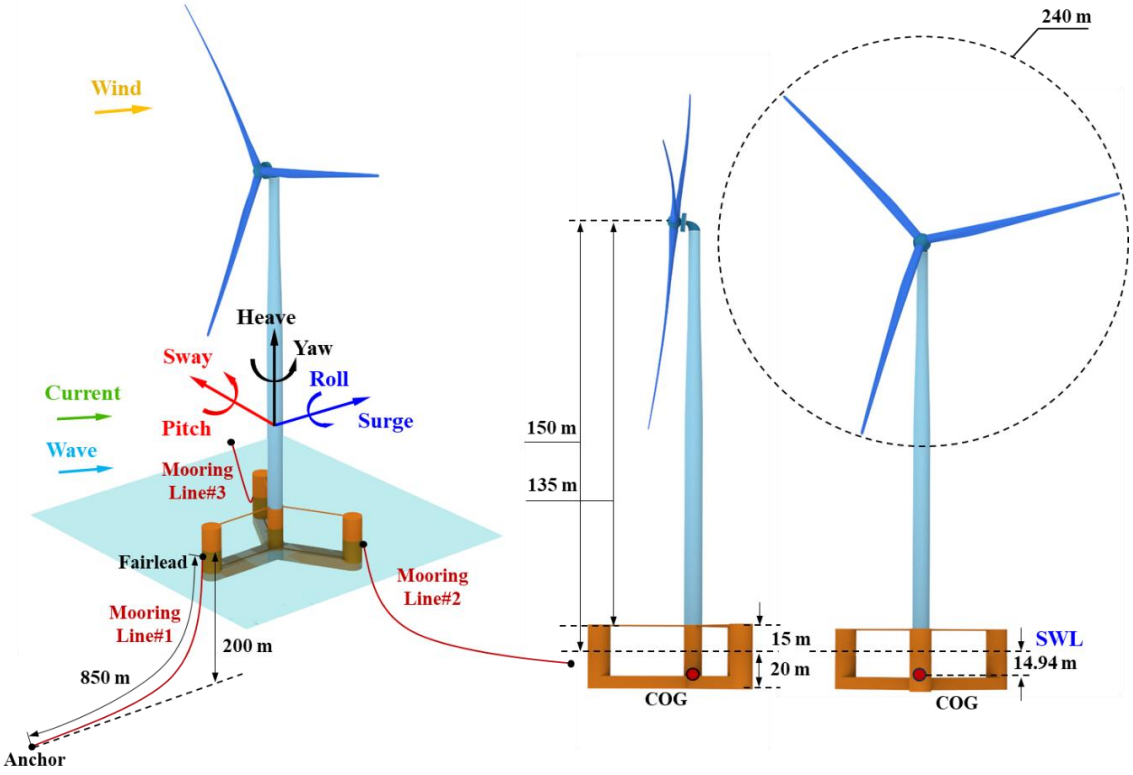

Fig. 1: The IEA 15MW FOWT model

2.2 Configuration of redundant mooring systems

The initial mooring system design for the VolturnUS-S FOWT adopts a non-redundant mooring system that deploys only one mooring line to limit the platform motion for each orientation. Mooring line breakage due to extreme loads or corrosion may cause unexpected disasters. Meanwhile, the nominal diameter of the initial mooring system is 0.185m and the mooring chain is R3-studless type. The unstretched length of each mooring line was 850m. Consequently, the translational motion of the platform under extreme environmental conditions would exceed the threshold that is set for the safety consideration of umbilical cable. To enhance the resilience of the whole FOWT against mooring failures event, two mooring system configurations are proposed as shown in Fig. 2. Each of the offset columns is connected to two or three mooring lines. The two configurations are hereinafter referred as the 6-Lines(6-L) mooring design and 9-Lines(9-L) mooring design, respectively. Regarding the

mooring chain type, the R4 studless chain is selected referring to the design experience of a practical project deployed in China. Since the number of mooring lines of the two redundant mooring systems is increased, the nominal diameter of each mooring line is reduced appropriately to obtain a proper extensional stiffness. The unstretched length and nominal diameter of the both redundant mooring systems are confirmed after running a series of simulations as per to the requirements of the design code for FOWTs [31]. The nominal diameter of the 6-L mooring configuration is 0.150m. The extensional stiffness and breaking load are respectively 1921.5MN and 20.16MN. The 9-L configuration employs the mooring line with a nominal diameter of 0.140m, since more cables are adopted. In both designs, the fairleads are placed at 14m below the still water line, the angle between the two mooring cables connected on the same column is 6 degrees for the 6-L mooring design. The corresponding angle is 3 degrees for the 9-L mooring design. The unstretched length of the mooring lines of these two configurations are 840m, which is consistent with the initial design of the IEA15 MW FOWT. The cross-sectional parameters for the two mooring types are provided in Table 3.

Table 3: Summary of the properties of the two redundant mooring systems

Property	Value/Unit	
	6-L design	9-L design
Line type	R4 Studless	R4 Studless
Nominal diameter	150 mm	140 mm
Number of lines	6	9
Fairlead depth	14 m	14 m
Anchor depth	200 m	200 m
Extensional Stiffness	1921.5 MN	1673.8 MN
Unstretched length	840 m	840 m
Breaking tension	20.16 MN	19.64 MN

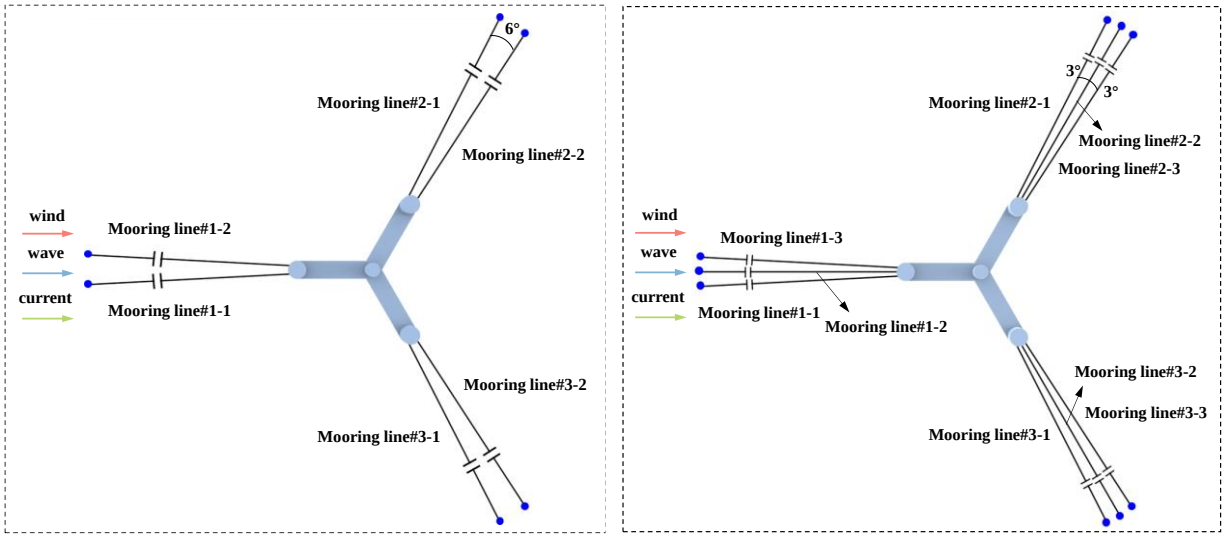

(a) 6-L mooring design (b) 9-L mooring design

Fig. 2: Top view of the new platform mooring system

3 *Development of fully coupled framework*

3.1 OpenF2A coupling framework

In 2020, Yang *et al.* [32-34] developed a fully coupled simulation framework (the so-called F2A) based on FAST and AQWA to examine the dynamics of the TELWIND concept that has two floaters. The FAST v7 was used to examine the aero-servo-elastic coupled effects of the wind turbine. However, the AeroDyn module incorporated within FAST v7 has several shortcomings in predicting the aerodynamic loads under turbulent wind conditions. For instance, the dynamic stall model used to correct the static lift and drag coefficients was unsatisfactory.

Therefore, this study has developed the fully coupled simulation framework by using OpenFAST v3.0.0 to more accurately predict the aerodynamic loads and structural dynamic responses of blades. The coupling between OpenFAST and AQWA is consistent with F2A. In this study, the Euler angle matrix is used for the motion transformation between the OpenFAST and AQWA. More details of the load conversion and motion transformation can be found in references [32, 35-36].

3.2 Validation of the fully coupled model

To validate the accuracy of the fully coupled simulation framework (OpenF2A), a comparative verification is performed against the results obtained by running fully independent OpenFAST simulations. Fig.3 presents the platform motions under turbulent wind condition calculated using OpenF2A and OpenFAST, respectively. It is noted that the dynamics of the platform and mooring system are examined entirely using different solvers, although the aero-servo-elastic responses predicted by these two tools are based on the same subroutines. The time-domain hydrodynamic loads and mooring dynamics corresponding to the OpenF2A results are examined in AQWA. The relevant results of OpenFAST are computed by the HydroDyn and MoorDyn that are built-in modules of OpenFAST program.

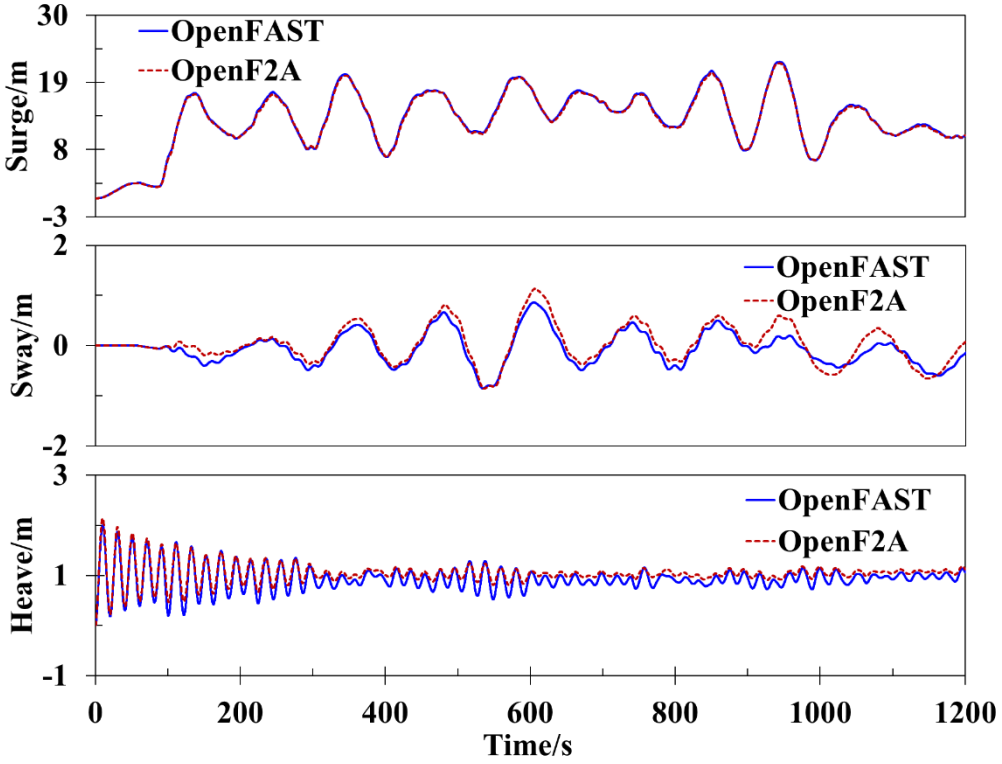

(a) Translational motions

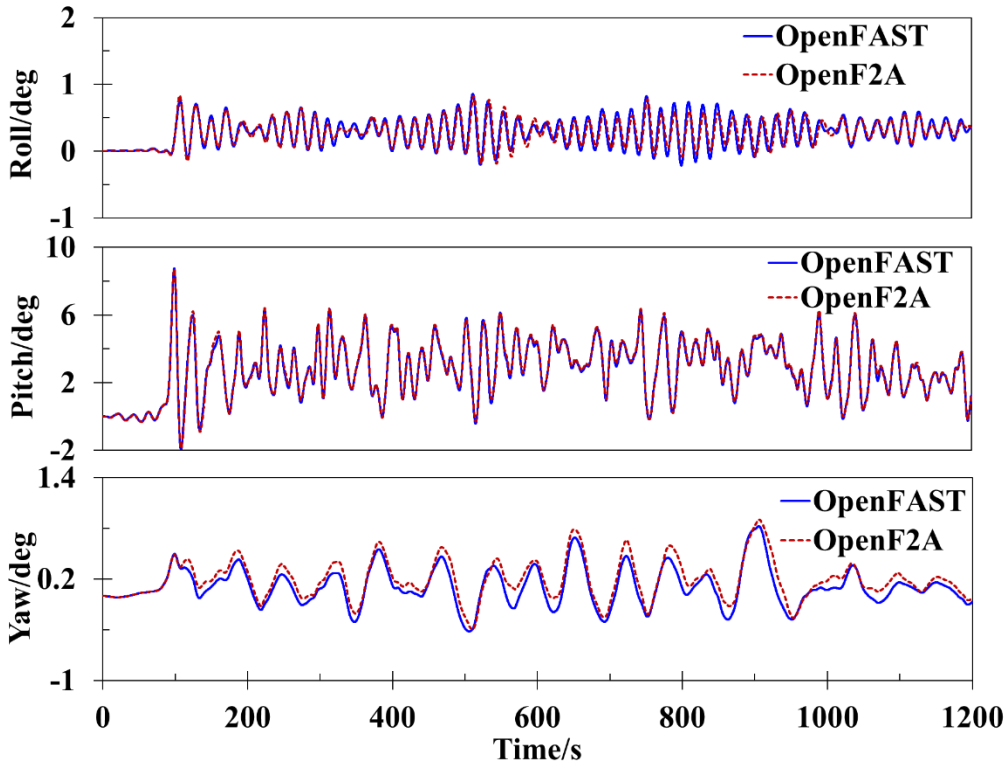

(b) Rotational motions

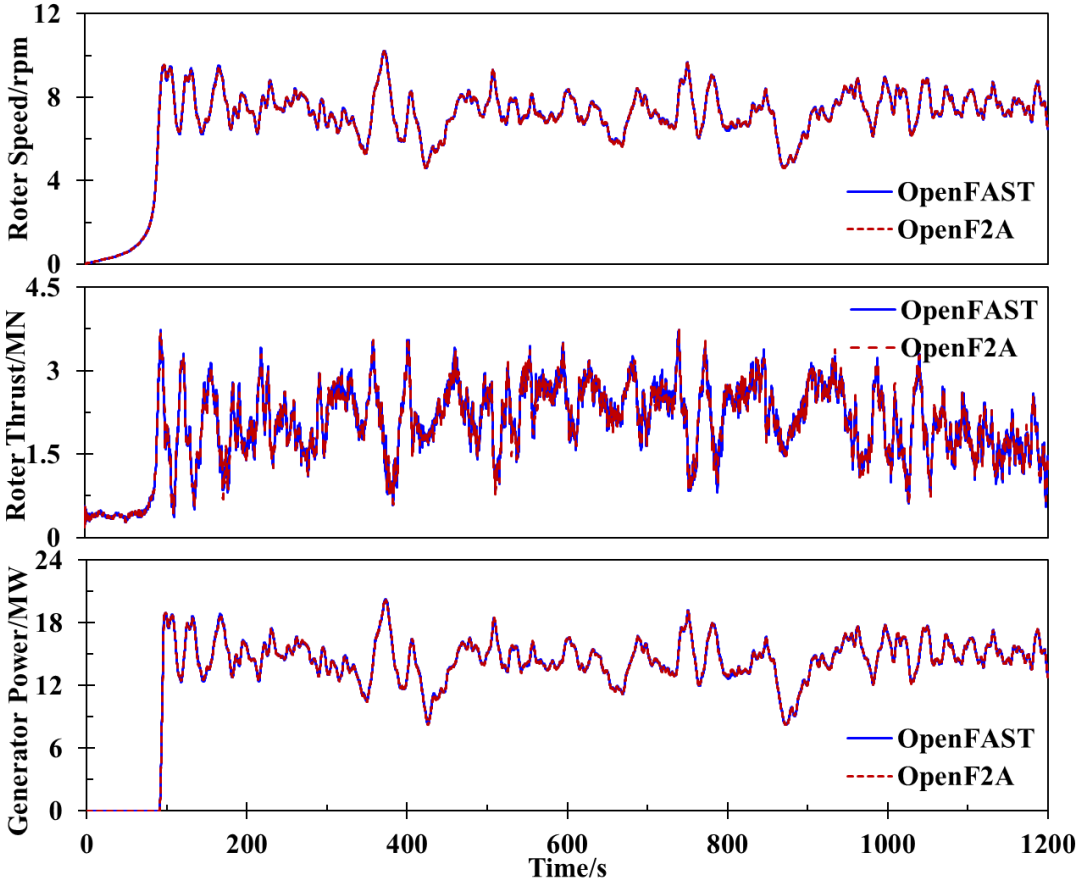

(c) Rotor dynamics

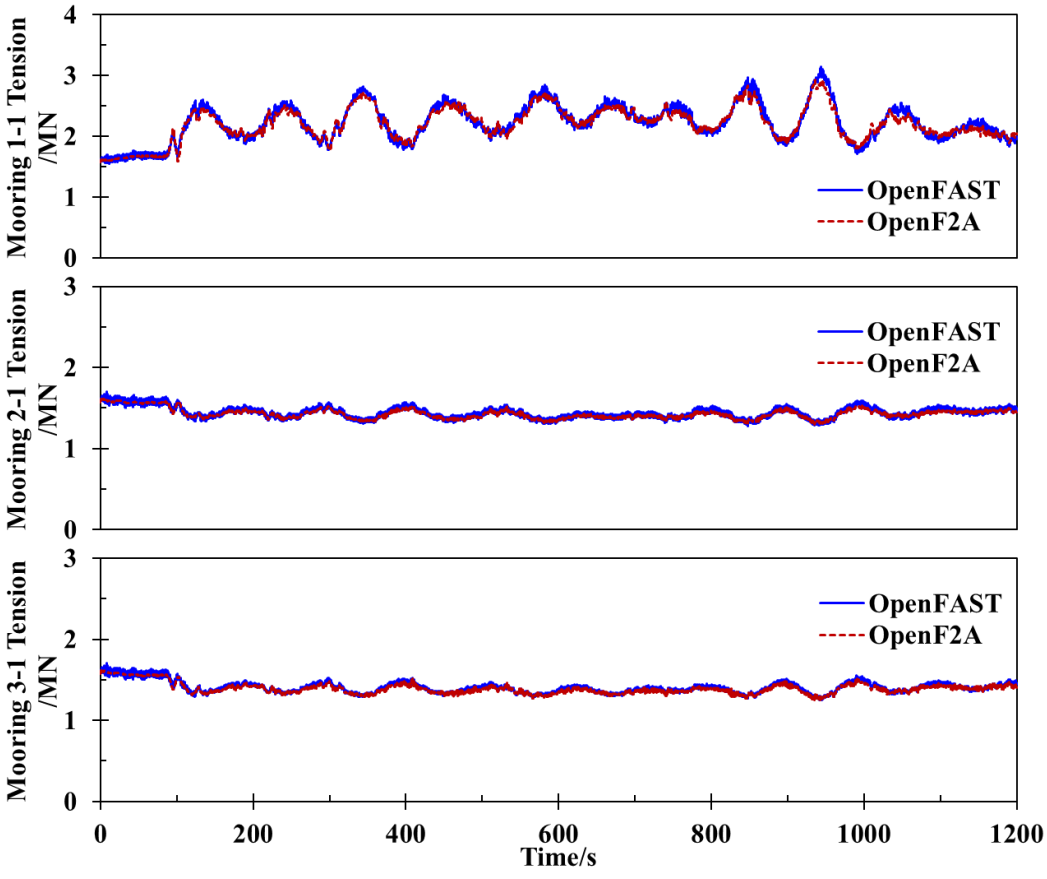

(d) Mooring tensions

Fig. 3: Comparisons between platform response OpenF2A and OpenFAST

The validation of the OpenF2A framework is carried out for a turbulent wind condition with an average speed of 12m/s. The simulation results of the OpenF2A and OpenFAST models show slight differences but with almost identical heave, sway, and roll motions. The maximum value of yaw, surge, and pitch motions are 0.90°, 22.08m and 8.75° when using OpenF2A. The maximum value of yaw, surge, and pitch motions are 0.83°, 22.34m and 8.75° for OpenFAST. The simulation results with two models are very similar. Meanwhile, the rotor dynamics and mooring tensions obtained by OpenF2A and OpenFAST are almost identical. These results have confirmed that OpenF2A is accurate in predicting the dynamic responses of the FOWT.

4 Analysis of simulation results for platform mooring failure

4.1 Definition of the simulation cases

To comprehensively study the stability and safety of the platform, it is necessary to investigate the response of platform and mooring tension variations under different operating conditions when mooring failure occurs. Table 4 presents the definitions of the environmental conditions of the load cases examined in this study. The wind turbine operating states include Operation (O) and Parked (P). All simulation conditions are categorized into three types: intact states, mooring breakage, and mooring lacking. When the wind turbine is in the O state, the rotor rotates and the generator operates to generate electricity. For this state, the wind speed is 11m/s, and the current speed at the mean sea level (MSL) is 0.81m/s. The significant wave height and spectral peak period are respectively 1.7m and 7.49s. When the wind turbine is in the P state, both the rotor and the generator are stopped. The corresponding wind, wave and current conditions are given as: mean wind speed of 50m/s, current speed at MSL of 2.5m/s, significant wave height of 11.65m and spectral peak period of 14.52s. The metocean data is shown in Table 5.

Fig. 4 presents the inflow angle to the FOWT. The inflow angle of 0° in the direction from the left to the right and the direction from the bottom to the top is the inflow angle of 90°. The mooring breakage occurred at the set time as given in Table 4. The operational state is defined following DLC1.1 and DLC1.7, while the parked state is defined in accordance with DLC6.1 and DLC6.6 of the IEC standard [37]. In case of the column “mooring breakage time/s”, where “-” means the mooring

lines are intact. “0” and “8000” denote the occurrence time of mooring breakage. The occurrence time of mooring breakage is set to 8000s so that the FOWT is operating stably when the mooring line failure happens. In addition, the simulation duration is set to 12000s, implying that the remaining time (4000s) is long enough to observe the transient and steady behavior of FOWT following a structure component failure. The time step of each simulation is 0.005s.

Table 4: Load cases for different environmental conditions

Mooring state	Load Case	Inflow angle/deg	Operational states	Mooring design	Mooring breakage ID	Mooring Breakage time/s
Intact state	LC1	0	P	6-L	-	-
	LC2	90	P	6-L	-	-
	LC3	180	P	6-L	-	-
	LC4	0	O	6-L	-	-
	LC5	90	O	6-L	-	-
	LC6	180	O	6-L	-	-
	LC7	0	P	9-L	-	-
	LC8	90	P	9-L	-	-
	LC9	180	P	9-L	-	-
	LC10	0	O	9-L	-	-
	LC11	90	O	9-L	-	-
	LC12	180	O	9-L	-	-
Mooring breakage	LC13	0	P	6-L	1-1	8000
	LC14	90	P	6-L	3-2	8000
	LC15	180	P	6-L	2-2	8000
	LC16	0	O	6-L	1-1	8000
	LC17	90	O	6-L	3-2	8000
	LC18	180	O	6-L	2-2	8000
	LC19	0	P	9-L	1-1	8000
	LC20	90	P	9-L	3-3	8000
	LC21	180	P	9-L	2-3	8000
	LC22	0	O	9-L	1-1	8000
	LC23	90	O	9-L	3-3	8000
	LC24	180	O	9-L	2-3	8000
Mooring lacking	LC25	0	P	6-L	1-1	0
	LC26	90	P	6-L	3-2	0
	LC27	180	P	6-L	2-2	0
	LC28	0	O	6-L	1-1	0
	LC29	90	O	6-L	3-2	0
	LC30	180	O	6-L	2-2	0
	LC31	0	P	9-L	1-1	0
	LC32	90	P	9-L	3-3	0
	LC33	180	P	9-L	2-3	0

LC34	0	O	9-L	1-1	0
LC35	90	O	9-L	3-3	0
LC36	180	O	9-L	2-3	0

Table 5: The metocean data

Operational states	Wind speed/(m/s)	Wave height/m	Spectral peak period/s	Current speed/(m/s)
O	11	1.70	7.49	0.81
P	50	11.65	14.52	2.5

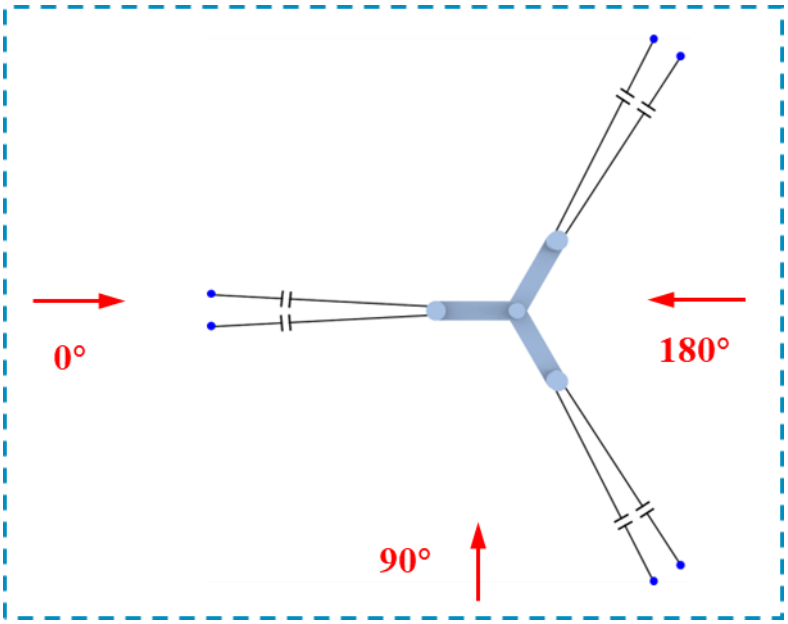

(a) The 6-L design

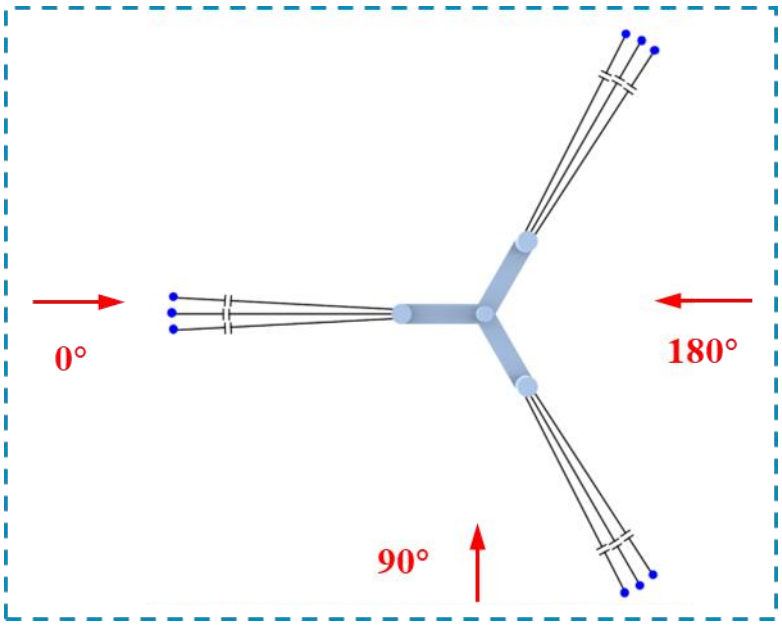

(b) The 9-L design

Fig. 4: Direction of wind, wave and current under simulated working conditions

4.2 Simulation results of mooring breakage scenarios

4.2.1 Results of rotational motions of platform

The rotational motions of platform in the O state are depicted in Fig. 5 under LC 16 and LC 22, in which the wind speed is 11m/s and current speed is 0.81m/s with 0° inflow angle. In LC 16, the mooring design is 6-L and the broken mooring is line#1-1. In LC 22, the mooring design is 9-L and the broken mooring is line#1-1.

As shown in Fig. 5-(a), the maximum value of roll under line#1-1 breakage with 6-L design is 0.64° and the maximum value of roll under the intact case with 6-L design is 0.64°. When mooring design is 9-L, the maximum value of roll under line#1-1 breakage is 0.60° and the maximum value of roll under the intact case is 0.60°. After mooring breakage, the maximum value of roll has not changed under both 6-L and 9-L designs. This indicated that the platform roll almost has not changed when mooring failure occurs during the power production phase.

As shown in Fig. 5-(b), the maximum value of pitch under line#1-1 breakage with 6-L design is 5.79° and the maximum value of pitch under the intact case with 6-L design is 5.06°. After mooring breakage, the maximum value of pitch has increased by about 14.33% with 6-L design. When mooring design is 9-L, the maximum value of pitch under line#1-1 breakage is 5.46° and the maximum value of pitch under the intact case is 4.89°. After mooring breakage, the maximum value of pitch has increased by about 11.83%. The platform pitch shows a slight increase following mooring failure, but the magnitude of this increase is minimal. In contrast, the increase in pitch under the 9-L design is even smaller.

It is observed that the effect of mooring failure to the rotational motions of platform is minimal, especially to the roll. Besides, comparing the curves of the two mooring designs, the roll motion of platform in the 9-L design is slightly larger than 6-L design and the pitch motion of platform is slightly lower.

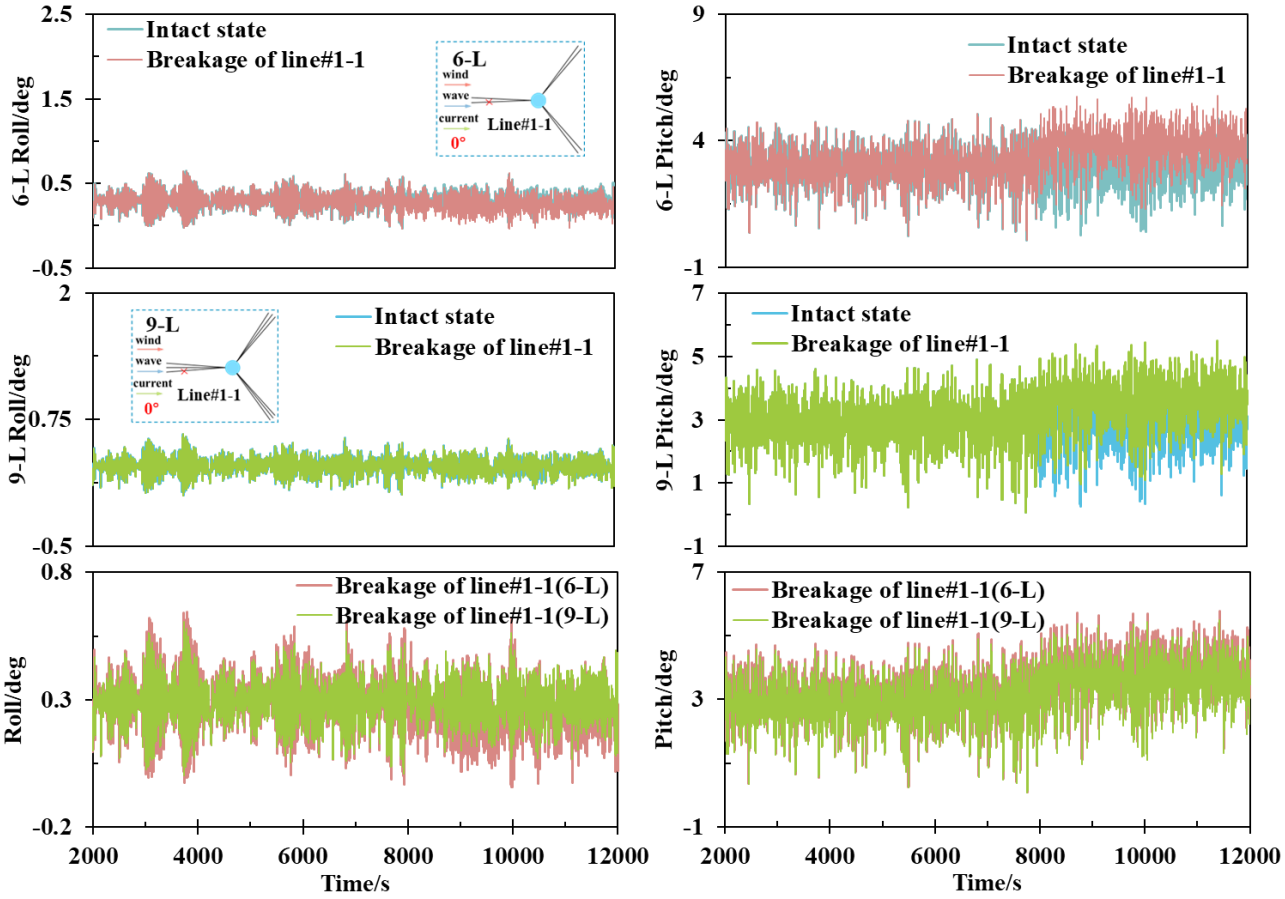

(a) Platform roll (b) Platform pitch

Fig. 5: The rotational motions of platform motions in O state

The rotational motions of platform response results in the P state are depicted in Fig. 6 under LC 13 and LC 19 in which the wind speed is 50m/s and current speed is 2.5m/s with 0° inflow angle. In LC 13, the mooring design is 6-L design and the broken mooring is line#1-1. In LC 19, the mooring design is 9-L design and the broken mooring is line#1-1.

As shown in Fig. 6-(a), the maximum value of roll under line#1-1 breakage with 6-L design is 0.51°and the maximum value of roll under the intact case with 6-L design is 0.33°. After mooring breakage, the maximum value of roll has increased by about 53.30% under 6-L design. When the mooring design is 9-L, the maximum value of roll under line#1-1 breakage is 4.11°. In this case, the maximum of roll has not changed.

As shown in Fig. 6-(b), the maximum value of pitch under line#1-1 breakage with 6-L design is 7.82°and the maximum value of pitch under the intact case with 6-L design is 7.82°. When mooring design is 9-L, the maximum value of pitch under line#1-1 breakage is 8.94° and the maximum value of pitch under the intact case is 8.94°. The maximum of roll with both 6-L and 9-L has not changed.

The conclusions indicate that the effect of mooring failure due to the rotational motions of

platform is minimal during parked condition and is essentially the same as during power production.

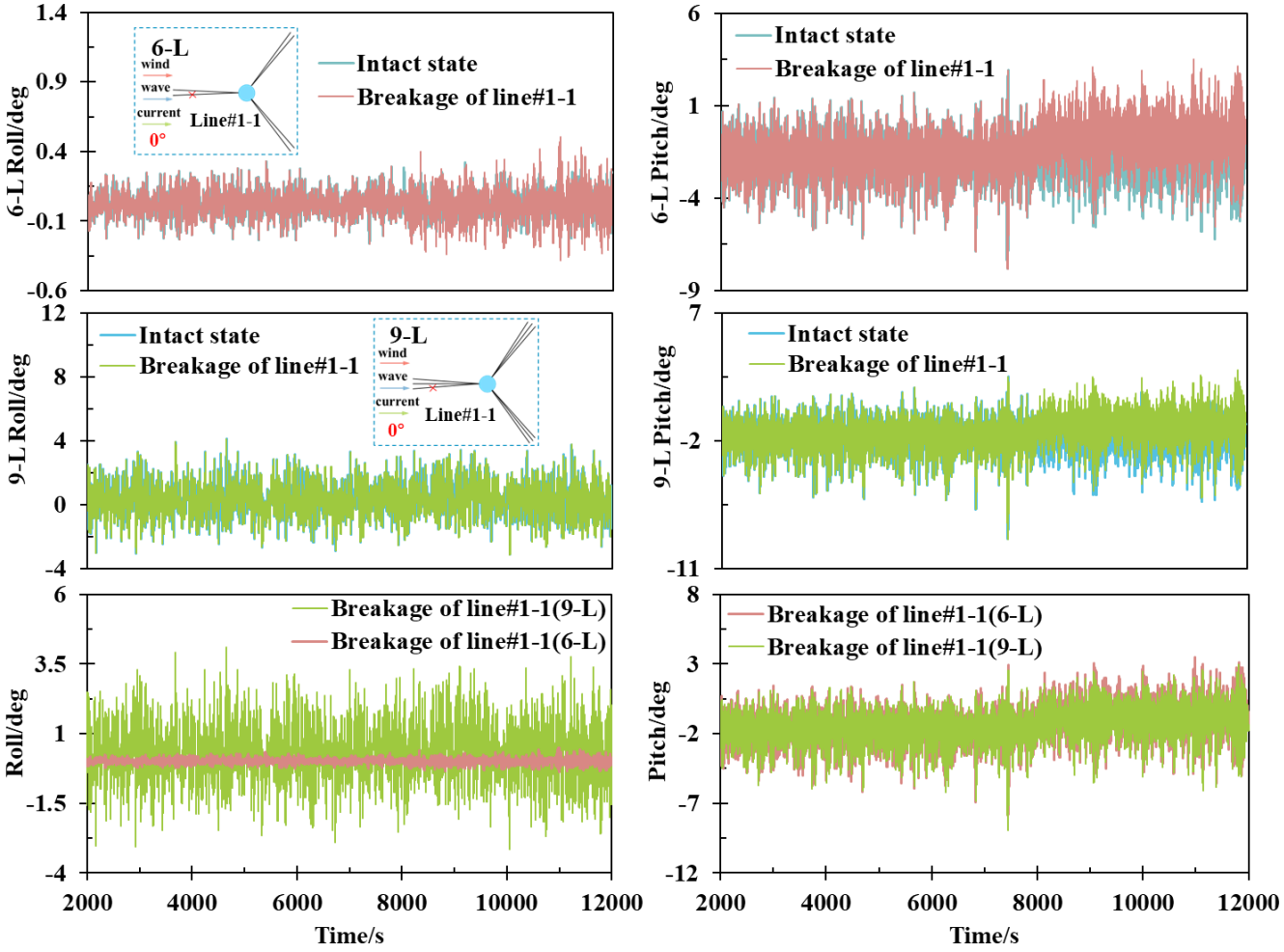

(a) Platform roll (b) Platform pitch

Fig. 6: The rotational motions of platform response results in P state

Table 6 presents the changes to platform rotational motion under all the case, where rotation in Table 6 is calculated as follows:

$$Rotation = \sqrt{Roll^2 + Pitch^2} \tag{4}$$

As shown in Table 6, all the peaks of rotational motion appeared under line#1-1 breakage at 0° inflow angle. The maximum of rotation with 6-L design is 5.79° in the O state. While with 9-L design in the O state, the maximum of rotation decreases to 5.47°. When in the P state, the maximum of rotation is 7.82° with 6-L design and the maximum of rotation is 8.96° with 9-L design. When a single mooring breaks, the 9-L design can reduce the maximum rotational motion under the power generation case compared with 6-L design. On the contrary, the 9-L design will increase the rotational motions of platform under the parked case compared with 6-L design. This phenomenon is the most pronounced when the inflow angle is 0°. But the effect of mooring failure to the rotational motion of platform is minimal under both 6-L and 9-L design.

306 It is found that that the maximum values under different inflow angles do not vary significantly.
307 The conclusions at a 0° inflow angle are applicable to other inflow angles. The comparison of
308 rotational motions at different inflow angles is shown in the Fig. 7.

309 Table 6: Maximum value of rotational and translational motions under 6-L and 9-L designs

Mooring breakage ID	Inflow angle (deg)	O/P States	Mooring design	Rotation (deg)	Translation (m)
1-1	0	O	6-L	5.82	28.52
3-2	90	O	6-L	5.73	30.69
2-2	180	O	6-L	5.60	32.67
Intact	0	O	6-L	5.10	13.76
Intact	90	O	6-L	5.16	16.34
Intact	180	O	6-L	5.14	18.50
1-1	0	P	6-L	7.84	38.91
3-2	90	P	6-L	8.88	50.82
2-2	180	P	6-L	6.94	56.22
Intact	0	P	6-L	7.83	28.59
Intact	90	P	6-L	8.28	38.27
Intact	180	P	6-L	6.90	47.79
1-1	0	O	9-L	5.50	19.10
3-3	90	O	9-L	5.44	20.52
2-3	180	O	9-L	5.30	22.08
Intact	0	O	9-L	4.92	11.30
Intact	90	O	9-L	5.01	12.84
Intact	180	O	9-L	5.02	14.42
1-1	0	P	9-L	9.84	31.67
3-3	90	P	9-L	9.14	39.86
2-3	180	P	9-L	7.64	45.63
Intact	0	P	9-L	9.84	26.88
Intact	90	P	9-L	8.72	33.87
Intact	180	P	9-L	7.64	42.97

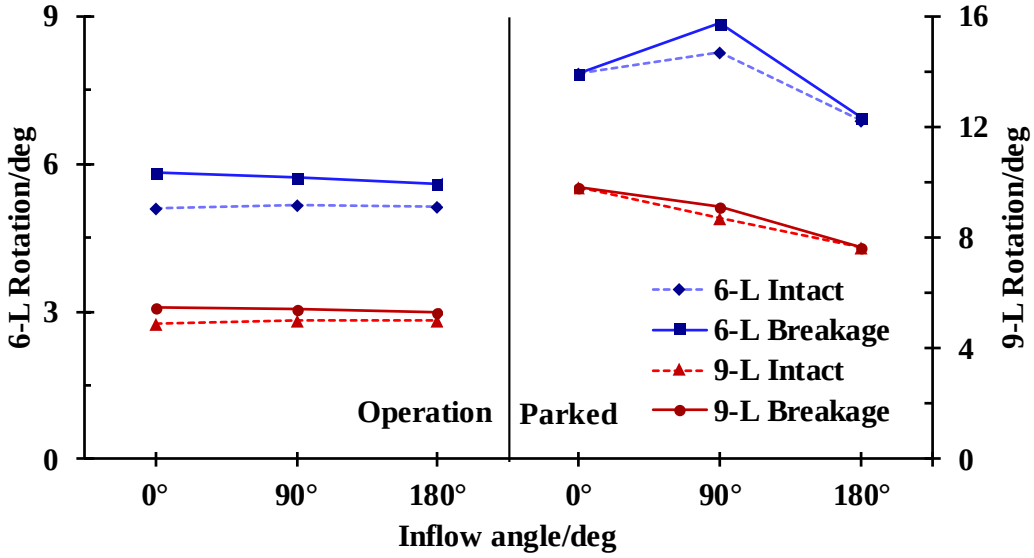

(a) The maximum of rotation

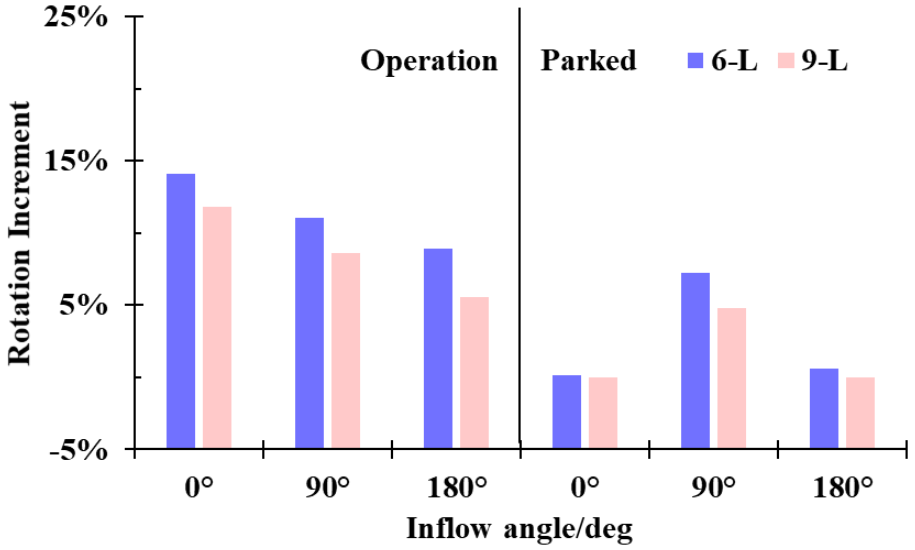

(b) The increment of rotation after mooring breakage

Fig. 7: Comparison of rotation motions under different inflow angles

4.2.2 Results of translational motions of platform

The translational motions of platform response results in the O state are depicted in Fig. 8 under LC 18 and LC 24 in which the wind speed is 11m/s and the current speed is 0.81m/s with 180° inflow angle. In LC 18, the mooring design is 6-L and the broken mooring is line#2-2. In LC 24, the mooring design is 9-L and the broken mooring is line#2-3.

As shown in Fig. 8-(a), the maximum value of surge under line#2-2 breakage with 6-L design is -29.71m and the maximum value of surge under the intact case with 6-L design is -18.5m. After mooring breakage, the maximum value of surge has increased by about 60.59% with 6-L design. When mooring design is 9-L, the maximum value of surge under line#2-3 breakage is -20.48m and

the maximum value of surge under the intact case is -14.42m. After mooring breakage, the maximum value of surge has increased by about 42.03% in 9-L design. It is indicated that the 9-L design can more effectively reduce the maximum value of surge than 6-L when the mooring failure occurred.

As shown in Fig. 8-(b), the maximum value of sway under line#2-2 breakage with 6-L design is -13.58m and the maximum value of sway under the intact case with 6-L design is -0.19m. After mooring breakage, the maximum value of sway has increased 13.39m with 6-L design. When mooring design is 9-L, the maximum value of sway under line#2-3 breakage is -8.26m and the maximum value of sway under the intact case is -0.17m. After mooring breakage, the maximum value of sway has increased 8.09m. The 9-L design can more effectively reduce the maximum value of sway at the same rate as surge.

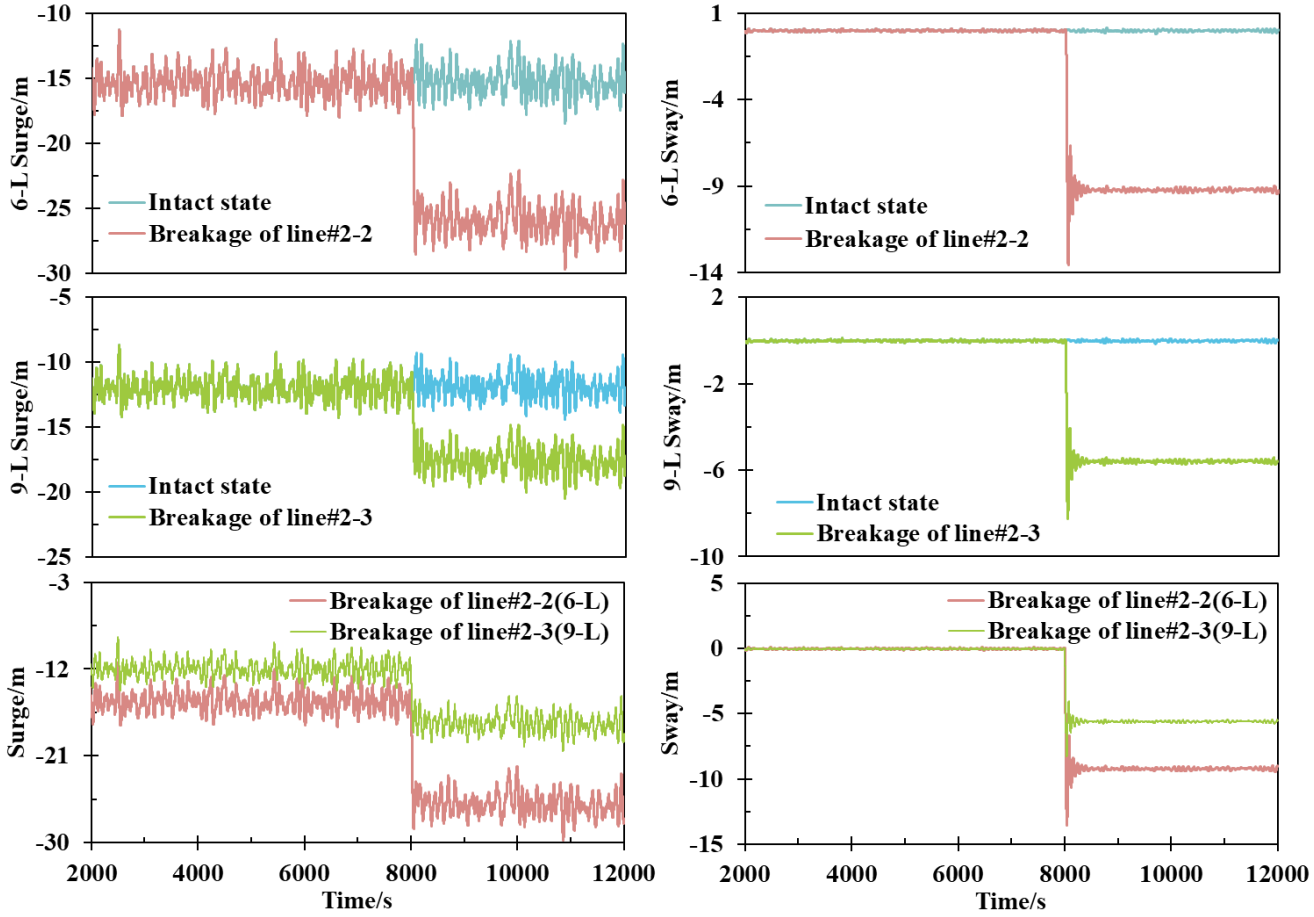

(a) Platform surge (b) Platform sway

Fig. 8: the translational motions of platform response results in O state

The translational motions of platform response results for the P state are depicted in Fig. 9 for LC 15 and LC 21 in which the wind speed is 50m/s and current speed is 2.5m/s with 0° inflow angle. In LC 15, the mooring design is 6-L and the broken mooring is line#2-2. In LC 21, the mooring design is 9-L and the broken mooring is line#2-3.

As shown in Fig. 9-(a), the maximum value of surge under line#2-2 breakage with the 6-L design is -55.07m and the maximum value of surge under the intact case with the 6-L design is -47.73m. After mooring breakage, the maximum value of surge has increased by about 15.38% with the 6-L design. When mooring design is the 9-L, the maximum value of surge under line#2-3 breakage is -45.03m and the maximum value of surge under the intact case is -42.93m. After mooring breakage, the maximum value of surge has increased by about 4.89% with the 9-L design. Both mooring designs can reduce the peak of surge in P state. However, the 6-L design is found to be more effective compared to others.

As shown in Fig. 9-(b), the maximum value of sway under line#2-2 breakage with the 6-L design is -11.30m and the maximum value of sway under the intact case with 6-L design is -2.41m. After mooring breakage, the maximum value of sway has increased by about 369.07% with the 6-L design. When mooring design is the 9-L, the maximum value of sway under line#2-3 breakage is -7.35m and the maximum value of sway under the intact case is -1.95m. After mooring breakage, the maximum value of sway has increased by about 277.08%. The conclusions indicate that the sway motion are the same as surge motion with 6-L and 9-L designs. This indicated that the 6-L design can more effectively reduce the maximum value of translational motions in P state.

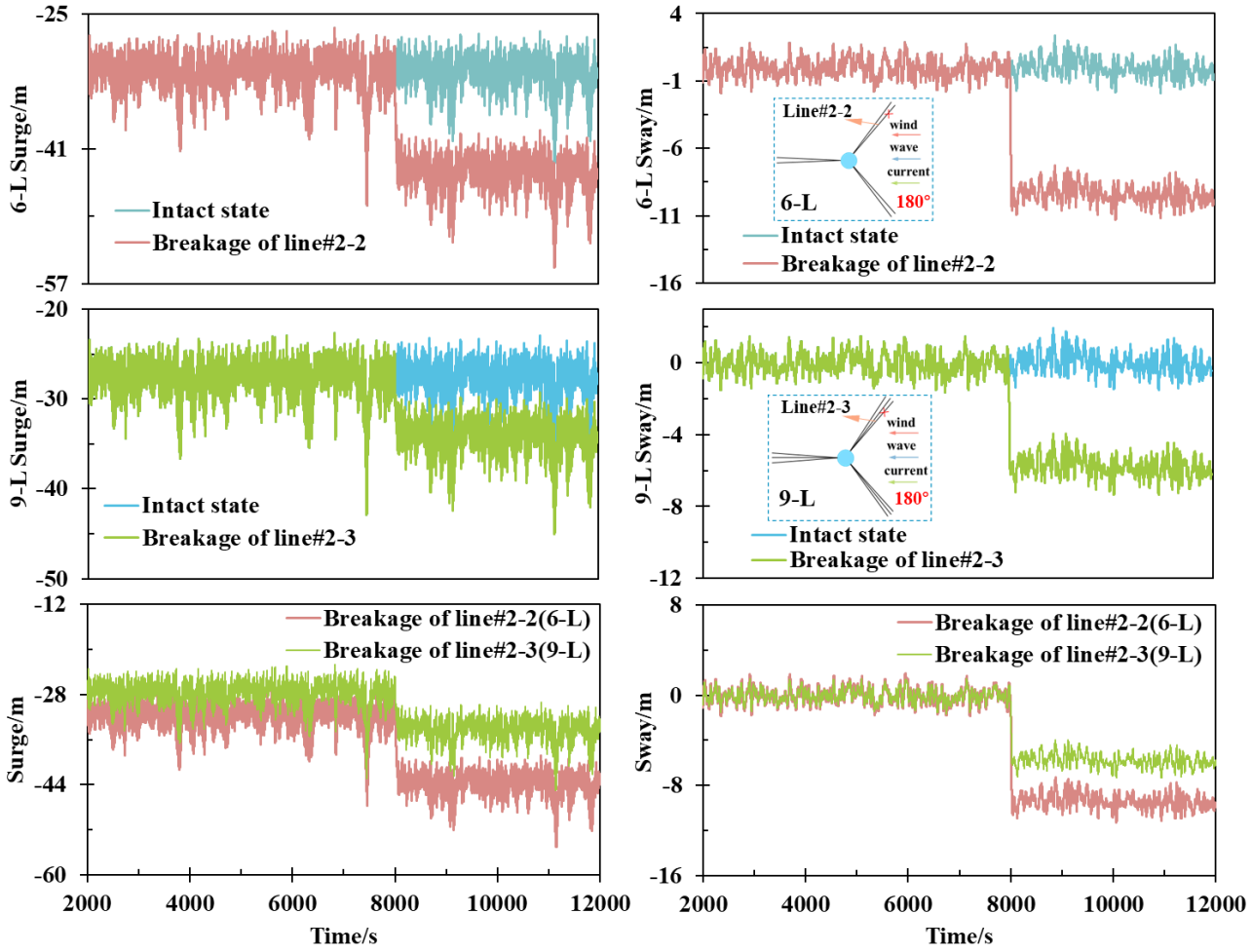

(a) Platform surge (b) Platform sway

Fig. 9: The translational motions of platform in the P state

Table 6 presents the translational motion of platform variations under all the case, where the total translation in Table 6 is calculated as follows:

$$Translation = \sqrt{Surge^2 + Sway^2} \tag{5}$$

As shown in Table 6, the maximum response of translation with the 6-L design under line#2-2 breakage at 180° inflow angle is 31.25m in the O state. While with the 9-L design in the O state, the maximum value of translation under line#2-3 breakage at 180° inflow angle decreases to 21.22m. When in the P state, the maximum of translation is 55.83m with the 6-L design under line#2-2 breakage at 180° inflow angle and the peak of translation is 45.32m with the 9-L design under line#2-3 breakage at 180° inflow angle. When a single mooring breaks, the 9-L design can reduce the translational motions of platform under the power generation and parked cases compared with the 6-L design.

It is found that that the maximum values under different inflow angles do not vary significantly. The conclusions at a 0° inflow angle are applicable to other inflow angles. The comparison of

rotational motions at different inflow angles is shown in the Fig. 10.

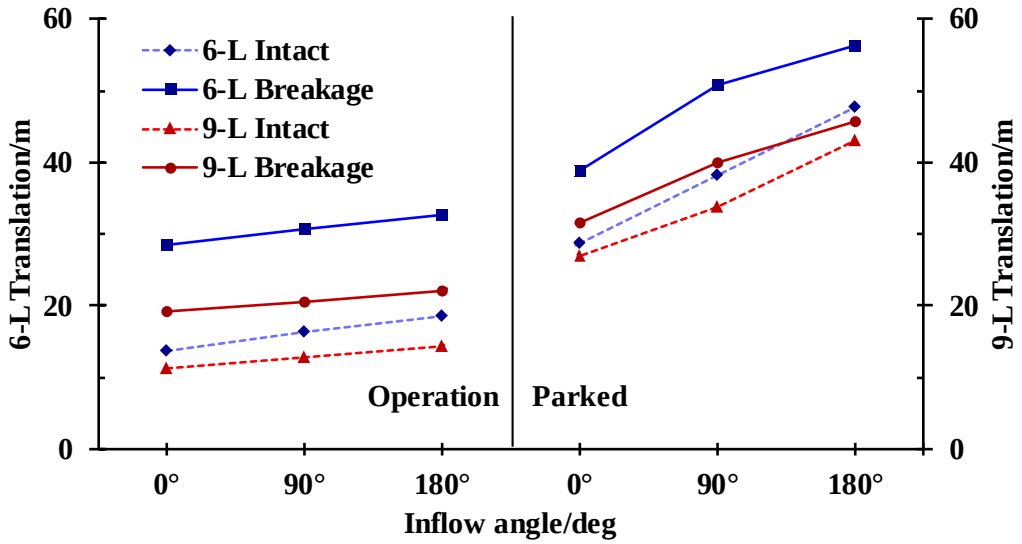

(a) The maximum of translation

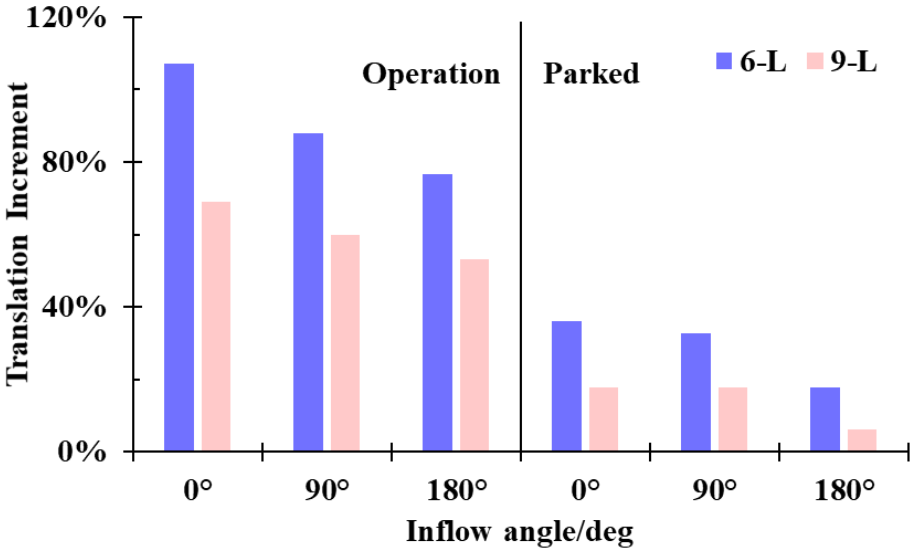

(b) The increment of translation after mooring breakage

Fig. 10: Comparison of translational motions under different inflow angles

4.2.3 Results of mooring tension

The platform response results for mooring fairlead tension in the O state are presented in Fig. 11 for LC 16 and LC 22. The maximum tension of outside fairlead(line#1-2) in the 0° direction under line#1-1 breakage and intact state with the 6-L design are 5.51MN and 3.09MN respectively. It is found that the maximum value of the fairlead tension in the outside mooring line has increased by 78.32%. The plausible reason to the abrupt tension increase is not only the stiffness loss due to mooring breakage, but also the snap load event in the remaining lines that are re-engaged immediately following a slack condition under mooring breakage scenarios. When line#1-1 breaks under 9-L

design, the maximum value of outside fairlead(line#1-3) tension in the 0° direction is 3.28MN. Meanwhile, under intact state is 2.46MN. It is found that the maximum value of outside fairlead tension has increased by 31.71%. Compared with the 6-L design, the 9-L design can effectively reduce the growth level for the maximum value of outside fairlead tension.

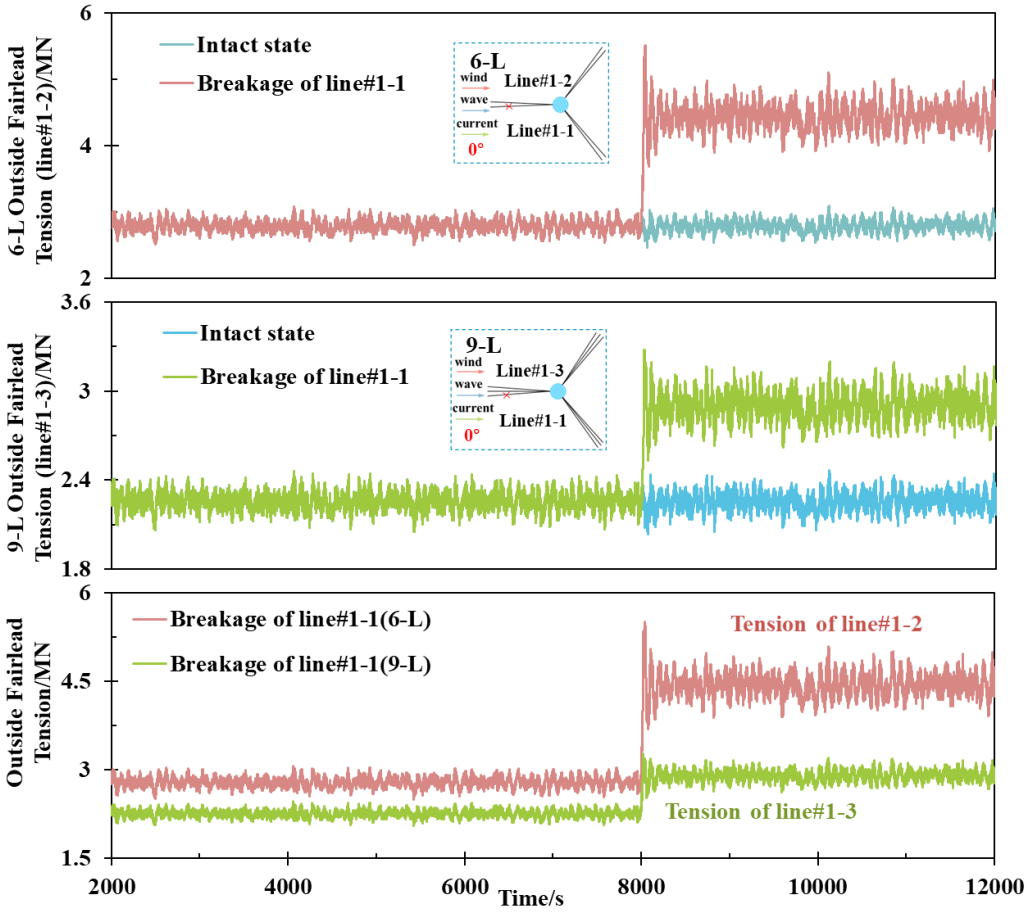

Fig. 11: Outside fairlead tension response results in O state

The mooring fairlead tension of platform response results in the P state are presented in Fig. 12 for LC 13 and LC 19. The maximum value of outside fairlead(line#1-2) tension in the 0° direction under line#1-1 breakage and intact state with the 6-L design are 16.95MN and 11.16MN, respectively. It is found that the maximum value of fairlead tension has increased by 51.88% due to occurrence of snap load event.

When line#1-1 breaks under the 9-L design, the maximum value of outside fairlead(line#1-3) tension in the 0° direction is 10.32MN, which is significantly smaller than the breaking force of the R4-150 mooring line(20.16MN). Meanwhile, under intact state is 8.57MN. It is found that the maximum fairlead tension is increased by 21.94%. The observations of the O state are consistent with the phenomenon of the P state.

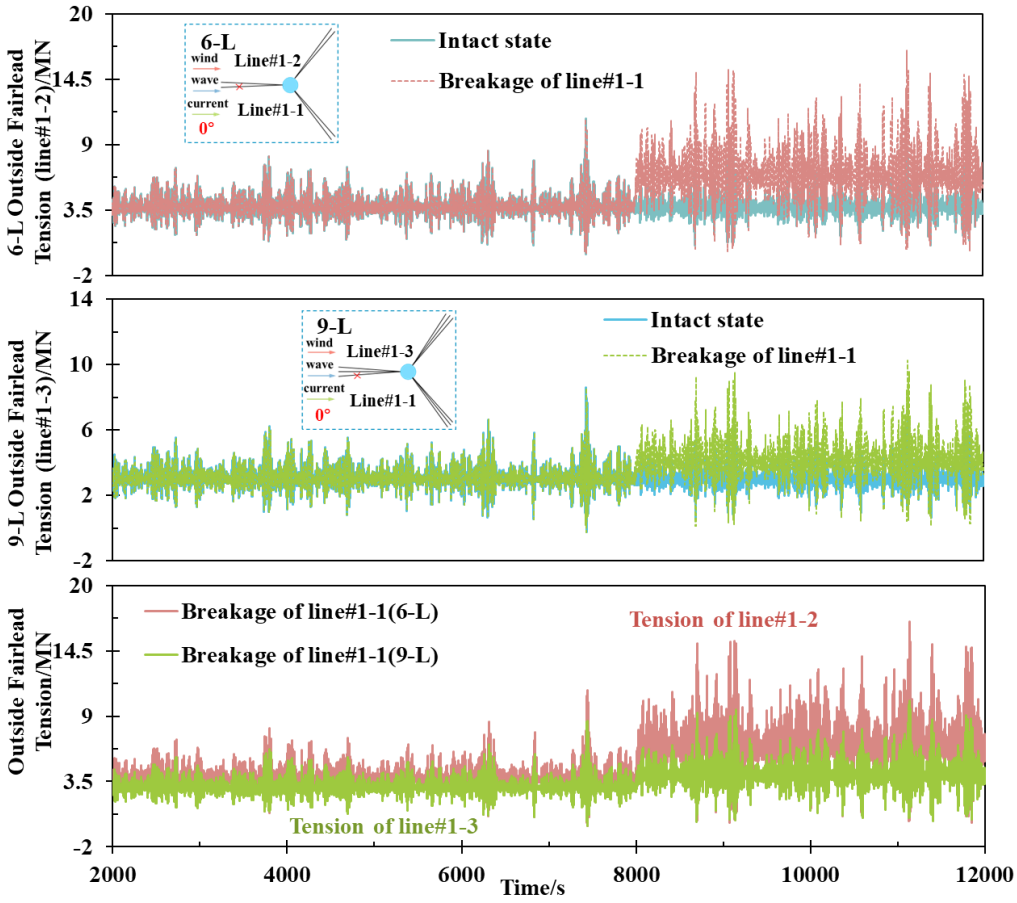

Fig. 12: Outside fairlead tension response results in P state

Table 8 and Table 9 present the maximum value of fairlead tensions under 6-L and 9-L designs. It is concluded that the 9-L design effectively reduces the growth level for the remaining fairlead tension in the same direction after mooring breakage. Besides, the maximum value of fairlead tension is most drastic at 0° inflow angle.

Table 8: Maximum value of fairlead tension under 6-L design

6-L	Mooring breakage ID	Inflow angle /deg	O/P States	Line# 1-1 (MN)	Line# 1-2 (MN)	Line# 2-1 (MN)	Line# 2-2 (MN)	Line# 3-1 (MN)	Line# 3-2 (MN)
LC16	1-1	0°	O	3.07	5.51	1.83	1.80	1.80	1.83
LC17	3-2	90°	O	2.26	2.17	1.61	1.63	5.20	2.97
LC18	2-2	180	O	1.56	1.56	4.75	2.74	2.76	2.61
LC4	-	0°	O	3.09	3.09	1.84	1.81	1.80	1.83
LC5	-	90°	O	2.26	2.17	1.61	1.63	2.90	3.01
LC6	-	180	O	1.56	1.56	2.59	2.74	2.76	2.61
LC13	1-1	0°	P	11.16	16.95	3.13	2.95	2.95	3.14
LC14	3-2	90°	P	4.11	3.79	2.09	2.20	15.18	10.67
LC15	2-2	180	P	1.78	1.96	10.39	8.43	8.14	6.64
LC1	-	0°	P	11.16	11.17	3.13	2.95	2.95	3.14
LC2	-	90°	P	4.11	3.79	2.09	2.20	9.68	10.67

LC3	-	180	P	1.95	1.96	7.00	8.43	8.14	6.64

Table 9: Maximum value of fairlead tension under 9-L design

9-L	Mooring breakage ID	Inflow angle /deg	States	Line# 1-1 (MN)	Line# 1-2 (MN)	Line# 1-3 (MN)	Line# 2-1 (MN)	Line# 2-2 (MN)	Line# 2-3 (MN)	Line# 3-1 (MN)	Line# 3-2 (MN)	Line# 3-3 (MN)
LC22	1-1	0°	O	2.46	3.21	3.28	1.61	1.57	1.58	1.59	1.58	1.61
LC23	3-3	90°	O	1.90	1.83	1.84	1.45	1.44	1.47	3.15	3.14	2.39
LC24	2-3	180	O	1.42	1.4	1.42	2.86	2.87	2.22	2.23	2.14	2.14
LC10	-	0°	O	2.46	2.42	2.46	1.61	1.58	1.59	1.59	1.58	1.61
LC11	-	90°	O	1.90	1.83	1.84	1.46	1.45	1.47	2.33	2.31	2.39
LC12	-	180	O	1.42	1.40	1.42	2.14	2.14	2.24	2.24	2.15	2.14
LC19	1-1	0°	P	8.57	10.17	10.28	2.78	2.65	2.62	2.77	2.81	2.96
LC20	3-3	90°	P	3.46	3.29	3.25	1.98	2.00	2.08	8.30	8.65	8.19
LC21	2-3	180	P	1.80	1.80	1.95	5.92	6.21	6.40	6.23	5.51	5.22
LC7	-	0°	P	8.57	8.34	8.59	2.78	2.65	2.62	2.77	2.81	2.96
LC8	-	90°	P	3.46	3.29	3.25	1.98	2.00	2.08	7.60	7.68	8.19
LC9	-	180	P	1.80	1.80	1.95	5.45	5.71	6.40	6.23	5.51	5.22

4.2.4 Transient effects of mooring breakage

Mooring fairlead tension experiences a sudden increase once a mooring failure occurs. In order to quantitatively evaluate the effects of sudden breakage of a mooring line, the mooring tensions under the sudden breakage scenario are compared with the results from intact state and mooring lacking condition. Fig. 13 presents the tensions in the mooring line adjacent to the broken line of the 6-L and 9-L configurations under the O state. It is observed that the fairlead tension reaches the peak value at the time of breakage for the both 6-L and 9-L mooring systems. The tension of the 6-L design is increased by 27.44% compared to the results of mooring lacking scenario. The corresponding increase is 10.47% for the 9-L design. The plausible reason to the more significant increase in 6-L mooring system is the occurrence of snap load event in the remaining mooring line. Moreover, snap load event is less likely to be happened in the 9-L mooring system, since there still two mooring lines left to limit the move of platform even a mooring line is fractured. The results indicated that the transient effects of mooring failure during power production need to be considered.

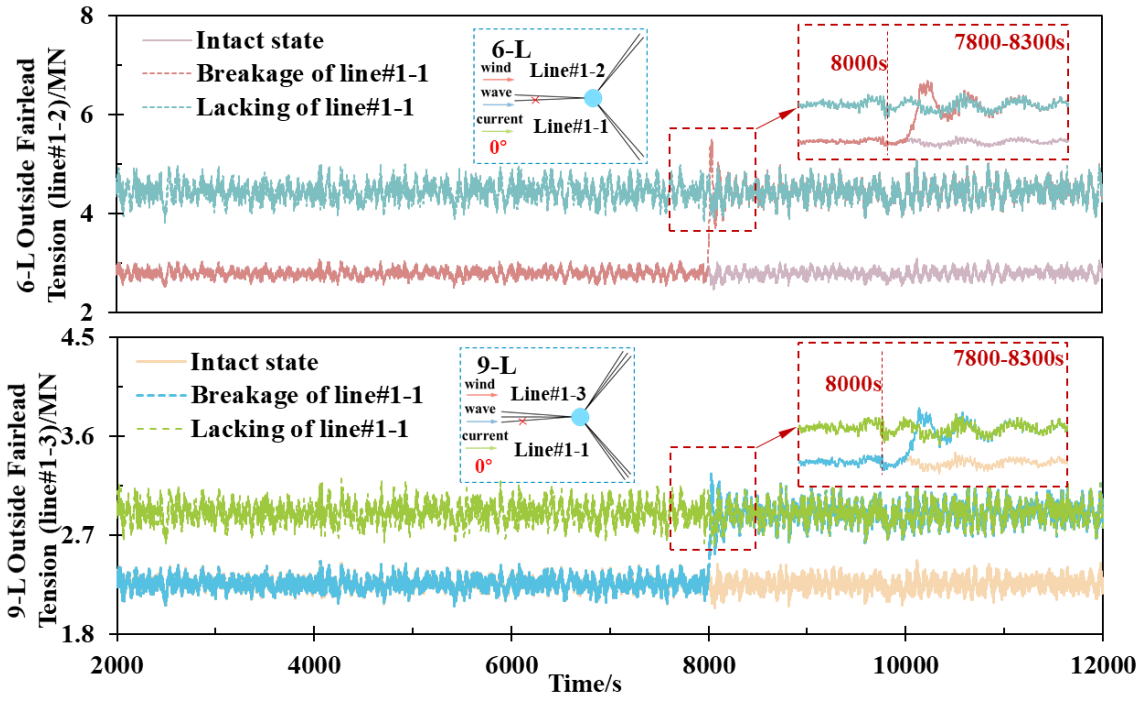

Fig. 13: Outside fairlead tension transient effect in O state

Fig. 14 presents the mooring tension variations when mooring breakages are occurred in the P state. Comparing the time-domain curves between mooring with and without failure conditions for the 6-L and 9-L mooring systems, it is found that the peak tension in the remaining mooring line is not observed at the breakage occurrence time. This is because the wind and wave conditions are very severe, resulting in large fluctuations in rotor thrust and platform motions, which are significant to the variation of mooring line tensions. Consequently, the mooring tension fluctuation is insensitive to the mooring breakage. The transient effects of mooring failure during parked conditions are minimal, which means that the transient effects caused by mooring failures can be simplified in engineering practical projects.

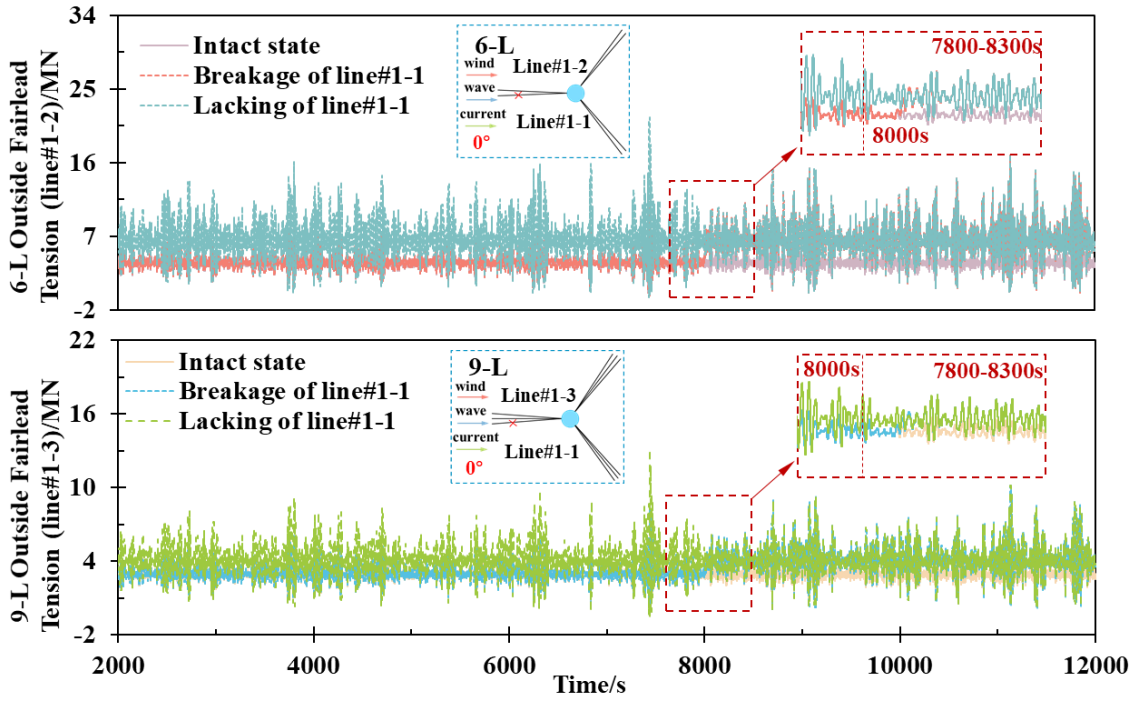

Fig. 14: Outside fairlead tension transient effect in P state

5. Conclusions

This paper has investigated the dynamic behaviors of the IEA 15MW FOWT subjected to a sudden mooring breakage of two redundant mooring system configurations. A fully coupled aero-hydro-servo-elastic tool (OpenF2A) is developed to conduct the simulations. The nonlinear dynamics and survivability of the FOWT in the case of a single mooring breakage under extreme and normal environmental conditions are investigated. The main findings of this study are summarized as follows:

(1) A fully coupled aero-hydro-servo-elastic simulation framework is developed based on AQWA and OpenFAST, which overcomes several shortcomings of the previously similar framework OpenF2A in predicting unsteady aerodynamic loads of the blades with ultra large deformation under the combined impact of wind, wave, and current loadings. The accuracy of the new framework in calculating the coupled dynamic responses of the platform and intact mooring system has been confirmed through comparisons against an established numerical analysis software package.

(2) The rotational motions of the platform are insensitive to the sudden mooring breakage under power production and parked states, while the translational motions of the platform and tension in the remaining mooring lines are significantly influenced by the fracture of a mooring line for both redundant mooring systems. The increase in platform drift exceeds

10m under power condition if the 6-L design is used than the 9-L design. The maximum tension in the adjacent mooring line is increased by 67.99% for the 6-L design under the power production due to occurrence of the snap load events.

(3) The transient effects induced by a sudden breakage of mooring line led to a sharp increase in the tension of the remaining mooring lines. This phenomenon is more significant for the 6-L design in power production as proved by the larger difference between the sudden breakage and lack of scenarios. The tension of the mooring breakage scenarios is increased by 27.44% and 10.47% compared to the results in mooring lacking cases for 6-L and 9-L mooring systems, respectively.

(4) The 9-L design shows a better stability than the 6-L design under the wind, waves, and current loadings. It effectively reduces platform displacement and decreases mooring tension when mooring breakage occurred. Meanwhile, the two designs can enhance mooring system redundancy too. However, the mooring utilization rate of the 6-L design is higher at 84.04%, surpassing that of the 9-L design. At the same time, the stability of the 6-L design meets the usage requirements. Considering the cost of mooring construction, the 6-L design proves to be more suitable for this type of platform.

Acknowledgements

The authors are grateful for the financial support from the National Key R&D Program of China (No. 2023YFE0102000), National Natural Science Foundation of China (Grant No.: 52101317), Ningbo Municipal Natural Science Foundation (Grant No.: 2023J091), Natural Science Foundation of Zhejiang Province (Grant No.: LQ22E090001), “Mechanics+” Interdisciplinary Top Innovative Youth Fund Project of Ningbo University (GC2024002) and National “111” Centre on Safety and Intelligent Operation of Sea Bridge (D21013). This study is also partially funded by the CREEI project (Contract No.: ZS-KJSD-20230005)

References

[1] Li, C., Ye, Z., Gao, W. (2012). Calculation and simulation of modern onshore and offshore wind turbines. Shanghai Science and Technology Press, 12-15.

[2] GWEC. Global offshore wind report 2024. 2024.

[3] Xiaohui, L. I. U., Renjie, G. A. O., & Yu, X. U. E. (2020). Current situation and future development trend of floating offshore wind turbine. Distributed Energy Resources, 5(3), 39-46.

[4] Carbon Trust. (2021). Floating Wind Joint Industry Project Phase III Summary Report. Retrieved from https://www.carbontrust.com/resources/floating-wind-joint-industry-project-phase-iii-summary-report.

[5] Bagbanci, H. (2011). Dynamic analysis of offshore floating wind turbines. Naval Architecture and Marine Engineering, Technical University of Lisbon.

[6] Ren, Y., Shi, W., Venugopal, V., Zhang, L., & Li, X. (2024). Experimental study of tendon failure analysis for a TLP floating offshore wind turbine. Applied Energy, 358, 122633.

[7] Gao, Z. T., Feng, X. Y., Zhang, Z. T., Liu, Z. L., Gao, X. X., Zhang, L. J., ... & Li, Y. (2022). A brief discussion on offshore wind turbine hydrodynamics problem. Journal of Hydrodynamics, 34(1), 15-30.

[8] Zhao, Z., Wang, W., Shi, W., & Li, X. (2020, December). Effects of second-order hydrodynamics on an ultra-large semi-submersible floating offshore wind turbine. In Structures (Vol. 28, pp. 2260-2275).

[9] Tang, Y., Hu, J., & Liu, L. (2011, January). Study on the dynamic response for floating foundation of offshore wind turbine. In International Conference on Offshore Mechanics and Arctic Engineering (Vol. 44373, pp. 929-933).

[10] Ye, X., Zhang, L., Wu, H., & Zhao, J. (2012). Influence of platform motion response on aerodynamic performance of floating offshore wind turbine. Huazhong Keji Daxue Xuebao(Ziran Kexue Ban)/ Journal of Huazhong University of Science and Technology(Nature Science Edition), 40(3).

[11] Spearman, D.K.; Strivens, S.; Matha, D.; Cosack, N.; Macleay, A.; Regelink, J.; Patel, D. (2020) Walsh, T. Floating Wind Joint Industry Project Phase II Summary Report. London, UK: Carbon Trust.

[12] Strivens, S.; Northridge, E.; Evans, H.; Harvey, M.; Camp, T.; Terry, N. (2021) Floating Wind Joint Industry Project Phase III Summary Report. London, UK: Carbon Trust.

[13] Siddiqui, N. A., & Ahmad, S. (2001). Fatigue and fracture reliability of TLP tethers under random loading. Marine structures, 14(3), 331-352.

[14] Yang, Y., Bashir, M., Li, C., & Wang, J. (2021). Investigation on mooring breakage effects of a 5 MW barge-type floating offshore wind turbine using F2A. Ocean Engineering, 233, 108887.

[15] Yang, C. K., & Kim, M. H. (2010). Transient effects of tendon disconnection of a TLP by hull–tendon–riser coupled dynamic analysis. Ocean Engineering, 37(8-9), 667-677.

[16] Kim, M. H., & Zhang, Z. (2009). Transient effects of tendon disconnection on the survivability of a TLP in moderate-strength hurricane condition. International Journal of Naval Architecture and Ocean Engineering, 1(1), 13-19.

[17] Yang, C. K., Padmanabhan, B., Murray, J., & Kim, M. H. (2008). The transient effect of tendon disconnection on the global motion of ETLP. In ASME 2008 27th International Conference on Offshore Mechanics and Arctic Engineering. American Society of Mechanical Engineers, Estoril, Portugal.

[18] Li, Y., Zhu, Q., Liu, L., & Tang, Y. (2018). Transient response of a SPAR-type floating offshore wind turbine with fractured mooring lines. Renewable Energy, 122, 576-588.

[19] Bai, X., Kong, L., Ji, C. (2018). Motion Response Characteristics of Semi-submersible Platform under Partial Mooring Failure, Ship Engineering, 40(06), 100-105.

[20] Ren, Y., Venugopal, V., & Shi, W. (2022). Dynamic analysis of a multi-column TLP floating offshore wind turbine with tendon failure scenarios. Ocean engineering, 245, 110472.

[21] Ma, G., Zhong, L., Zhang, X., Ma, Q., & Kang, H. S. (2020). Mechanism of mooring line breakage of floating offshore wind turbine under extreme coherent gust with direction change condition. Journal of Marine Science and Technology, 25, 1283-1295.

[22] Yang, R. Y., Chuang, T. C., Zhao, C., & Johanning, L. (2022). Dynamic response of an offshore floating wind turbine at accidental limit states—mooring failure event. Applied Sciences, 12(3), 1525.

[23] Bae, Y. H., Kim, M. H., & Kim, H. C. (2017). Performance changes of a floating offshore wind turbine with broken mooring line. Renewable Energy, 101, 364-375.

[24] Wu, H., Zhao, Y., He, Y., Shao, Y., Mao, W., Han, Z., ... & Jiang, Z. (2021). Transient response of a TLP-type floating offshore wind turbine under tendon failure conditions. Ocean Engineering, 220, 108486.

[25] Subbulakshmi, A., & Verma, M. (2023). Transient response reduction of floating offshore wind turbine subjected to sudden mooring line failure. Ocean Engineering, 271, 113702.

[26] He Saiping.(2017) Dynamic Tension Analysis of the Mooring Line of the Offshore Floating Wind Turbine. AFORE, 296-296.

[27] Piscopo, V., & Scamardella, A. (2021). Comparative study among non-redundant and redundant stationkee** systems for floating offshore wind turbines on intermediate water depth. Ocean Engineering, 241, 110047.

[28] Niranjan, R., & Ramisetti, S. B. (2023). Dynamic response of 15 MW floating wind turbine with non-redundant and redundant mooring systems under extreme and accidental conditions. Journal of Offshore Mechanics and Arctic Engineering, 145(6), 062002.

[29] Jonkman, J. M., & Buhl Jr, M. L. (2005). FAST user's guide. National Renewable Energy Laboratory (NREL), Technical Reports (No. NREL/EL-500-38230), Golden, United States.

[30] Gaertner, E., Rinker, J., Sethuraman, L., Zahle, F., Anderson, B., Ananthan, S., ... & Abbas, N. (2020). Definition of the IEA 15-Megawatt Offshore Reference Wind Turbine. Boulder, CO: National Renewable Energy Laboratory.

[31] China Classification Society. (2024). Rules for the Classification of Sea-going Steel Ships. Beijing, China: China Classification Society.

[32] Yang, Y., Bashir, M., Michailides, C., Li, C., & Wang, J. (2020). Development and application of an aero-hydro-servo-elastic coupling framework for analysis of floating offshore wind turbines. Renewable Energy, 161, 606-625.

[33] Yang, Y., Bashir, M., Wang, J., Michailides, C., Loughney, S., Armin, M., ... & Li, C. (2020). Wind-wave coupling effects on the fatigue damage of tendons for a 10 MW multi-body floating wind turbine. Ocean Engineering, 217, 107909.

[34] Yang, Y., Bashir, M., Michailides, C., Mei, X., Wang, J., & Li, C. (2021). Coupled analysis of a 10 MW multi-body floating offshore wind turbine subjected to tendon failures. Renewable Energy, 176, 89-105.

[35] Yang, Y., Fu, J., Shi, Z., Ma, L., Yu, J., Fang, F., ... & Li, C. (2023). Performance and fatigue analysis of an integrated floating wind-current energy system considering the aero-hydro-servo-elastic coupling effects. Renewable Energy, 216, 119111.

[36] Yang, Y., Shi, Z., Fu, J., Ma, L., Yu, J., Fang, F., ... & Yang, W. (2023). Effects of tidal turbine number on the performance of a 10 MW-class semi-submersible integrated floating wind-current system. Energy, 285, 128789.

[37] International Electrotechnical Commission. (2019). IEC 61400-1: Wind turbines – Part 1: Design requirements (4th ed.). Geneva, Switzerland: IEC.